Contrib Mineral Petrol (2014) 167:1025
DOI 10.1007/s00410-014-1025-3

ORIGINAL PAPER

Building zoned ignimbrites by recycling silicic cumulates: insight from the 1,000 km^3 Carpenter Ridge Tuff, CO

Olivier Bachmann · Chad D. Deering · Peter W. Lipman · Charles Plummer

Received: 11 July 2013 / Accepted: 23 May 2014 / Published online: 10 June 2014

Abstract The ~1,000 km^3 Carpenter Ridge Tuff (CRT), erupted at 27.55 Ma during the mid-tertiary ignimbrite flare-up in the western USA, is among the largest known strongly zoned ash-flow tuffs. It consists primarily of densely welded crystal-poor rhyolite with a pronounced, highly evolved chemical signature (high Rb/Sr, low Ba, Zr, Eu), but thickly ponded intracaldera CRT is capped by a more crystal-rich, less silicic facies. In the outflow ignimbrite, this upper zone is defined mainly by densely welded crystal-rich juvenile clasts of trachydacite composition, with higher Fe–Ti oxide temperatures, and is characterized by extremely high Ba (to 7,500 ppm), Zr, Sr, and positive Eu anomalies. Rare mafic clasts (51–53 wt% SiO_2) with Ba contents to 4,000–5,000 ppm and positive Eu anomalies are also present. Much of the major and trace-element variations in the CRT juvenile clasts can be reproduced via in situ differentiation by interstitial melt extraction from a crystal-rich, upper-crustal mush zone, with the trachydacite, crystal-rich clasts representing the remobilized crystal cumulate left behind by the melt extraction process. Late recharge events, represented by the rare mafic clasts and high-Al amphiboles in some samples, mixed in with parts of the crystal cumulate and generated additional scatter in the whole-rock data. Recharge was important in thermally remobilizing the silicic crystal cumulate by partially melting the near-solidus phases, as supported by: (1) ubiquitous wormy/sieve textures and reverse zoning patterns in feldspars and biotites, (2) absence of quartz in this very silicic unit stored at depths of >4–5 km, and (3) heterogeneous melt compositions in the trachydacite fiamme and mafic clasts, particularly in Ba, indicating local enrichment of this element due mostly to sanidine and biotite melting. The injection of hot, juvenile magma into the upper-crustal cumulate also imparted the observed thermal gradient to the deposits and the mixing overprint that partly masks the in situ differentiation process. The CRT provides a particularly clear perspective on processes of in situ crystal-liquid separation into a lower crystal-rich zone and an upper eruptible cap, which appears common in incrementally built upper-crustal magma reservoirs of high-flux magmatic provinces.

Keywords Zoned ignimbrite · Magmatic differentiation · Supervolcanoes · Magmatism in the W USA · Gradients in magma chambers

Communicated by G. Moore.

Electronic supplementary material The online version of this article (doi:10.1007/s00410-014-1025-3) contains supplementary material, which is available to authorized users.

O. Bachmann (✉)
Institute of Geochemistry and Petrology, ETH Zürich, Clausiusstrasse 25, 8092 Zurich, Switzerland
e-mail: baolivie@ethz.ch; olivier.bachmann@erdw.ethz.ch

C. D. Deering
Department of Geological and Mining Engineering and Sciences, Michigan Technological University, Dow 630, Houghton, MI 49931-1295, USA

P. W. Lipman
Volcano Hazards Team, U.S. Geological Survey, MS910, 345 Middlefield Road, Menlo Park, CA 94025, USA

C. Plummer
Department of Earth and Space Sciences, University of Washington, Box 351310, Seattle, WA 98195-1310, USA

Introduction

Large-volume volcanic eruptions of silicic magma provide unique views of upper-crustal magma reservoirs; the rapid

evacuation of hundreds to thousands of cubic kilometers of magma allows for a snapshot of the state of the reservoir prior to eruption. Although some ignimbrites are compositionally homogeneous in bulk-rock composition (e.g., Dunbar et al. 1989; Lindsay et al. 2001; Bachmann et al. 2002; Folkes et al. 2011; Ellis and Wolff 2012), many show significant mineralogical and chemical variations from early to late-erupted material (e.g., Lipman 1967; Hildreth 1979, 1981; Worner and Schmincke 1984b). Two main *end-member* models have emerged to explain the origin of these compositional gradients in such ignimbrites: (1) mixing of two distinct magmas (many papers, but see in particular Dorais et al. 1991; Eichelberger et al. 2000) and (2) crystal–liquid separation and associated chemical fractionation (i.e., in situ differentiation; Lipman et al. 1966; Hildreth 1981; Bacon and Druitt 1988 among many others).

In an attempt to determine the relative contributions of mixing and in situ differentiation in the generation of such large-volume zoned ignimbrites, we have re-evaluated the petrology and geochemistry of one of the largest and most strongly zoned examples in the world, the ~1,000 km^3 Carpenter Ridge Tuff (CRT), which erupted ~27.55 My ago from the Bachelor caldera in the Southern Rocky Mountain volcanic field (SRMVF; Lipman 2007). The outflow sheet is dominated by densely welded crystal-poor rhyolite, but the thickly ponded intracaldera accumulation is capped by a comparatively low-volume zone of crystal-rich trachydacite, the Mammoth Mountain Member (Lipman 2000). In the outflow ignimbrite, the analogous upper zone is defined by a discontinuous facies that contains crystal-rich, welded trachydacite fiamme and mafic clasts (Lipman 1975, 2000; Whitney et al. 1988; Dorais et al. 1991) with unusual bulk concentrations in certain trace elements (e.g., high Ba, Sr, Zr contents, but low Rb). We focused on characterizing the mineral and trace-element record in early and late-erupted material (pumice/scoria clasts when possible) in order to test a previously published hypothesis that suggested magma mixing between a crystal-poor silicic magma and a strongly alkalic recharge as the primary process leading to the observed compositional gradient in the CRT (Whitney et al. 1988; Dorais et al. 1991). We present an alternative model based on detailed examination of phenocrysts and re-evaluation of the major and trace-element chemistry. This model ties the different erupted compositions to a coherent differentiation scheme and is consistent with a process of in situ fractional crystallization governing the compositional variation within this large-volume silicic ash-flow tuff, although mixing with hotter recharge also played a role shortly before eruption.

Geologic setting

The earliest expression of magmatism in the San Juan locus of the SRMVF was growth of large andesitic stratovolcanoes (e.g., Steven and Lipman 1976; Lipman et al. 1978) that dominated volcanic activity from ~33.5 to 29.5 Ma. Around 30 Ma, more silicic magmas began to erupt, developing into large, caldera-forming events (oligocene ignimbrite flare-up episode; Steven and Lipman 1976; Lipman 2000, 2007). Multi-cyclic caldera clusters first developed in the SE and SW parts of the San Juan volcanic field, before focusing in the central caldera cluster, where the largest ignimbrites (including the CRT) erupted. The magmatic province is characterized by a high-K calc-alkaline trend and was likely a consequence of low-angle subduction under North America (Lipman 2007).

The 27.55-Ma CRT (Lipman and McIntosh 2008) is the second largest ash-flow sheet erupted from the central caldera cluster of the SRMVF. It formed the 25 × 30 km Bachelor caldera, which is nested inside the much larger La Garita caldera, the collapse structure of the preceding eruption (Fish Canyon Tuff) about 0.5 my earlier. The chemically and thermally zoned CRT contrasts with the two previous eruptions in the same area (both monotonous intermediates: the Masonic Park Tuff and the Fish Canyon Tuff) and is the first of four zoned ash-flow sheets from the central cluster (together with Wason Park, Rat Creek and Nelson Mountain Tuffs; see Lipman 2000, 2007 for additional information on these ignimbrites).

Sampling and analytical methods

In total, 16 samples were studied (Appendix 1 of ESM), including whole-rock XRF analyses of eight samples (Appendix 2 of ESM). Numerous additional whole-rock analyses, plotted in Figs. 1 and 2, were compiled by Lipman (2006) from previous studies. While relatively few, the new whole-rock analyses from this study represent key samples from (1) the exposed base of the CRT (crystal-poor rhyolite, CRT08-1), (2) a bulk-tuff sample (equivalent to the mixed sample of Dorais et al. 1991, CRT08-6), (3) crystal-rich fiamme from the outflow facies and the intracaldera Mammoth Mountain Member that show partial mingling with a more mafic recharge (CRT08-7 and CRT08-8, as well as CRT09-5), and (4) three more mafic scoria clasts (99L-10A, 99L-10B, and 99L-11). Analytical methods are summarized in Appendix 3 of ESM, and electron microprobe data are listed in Appendix 2 of ESM.

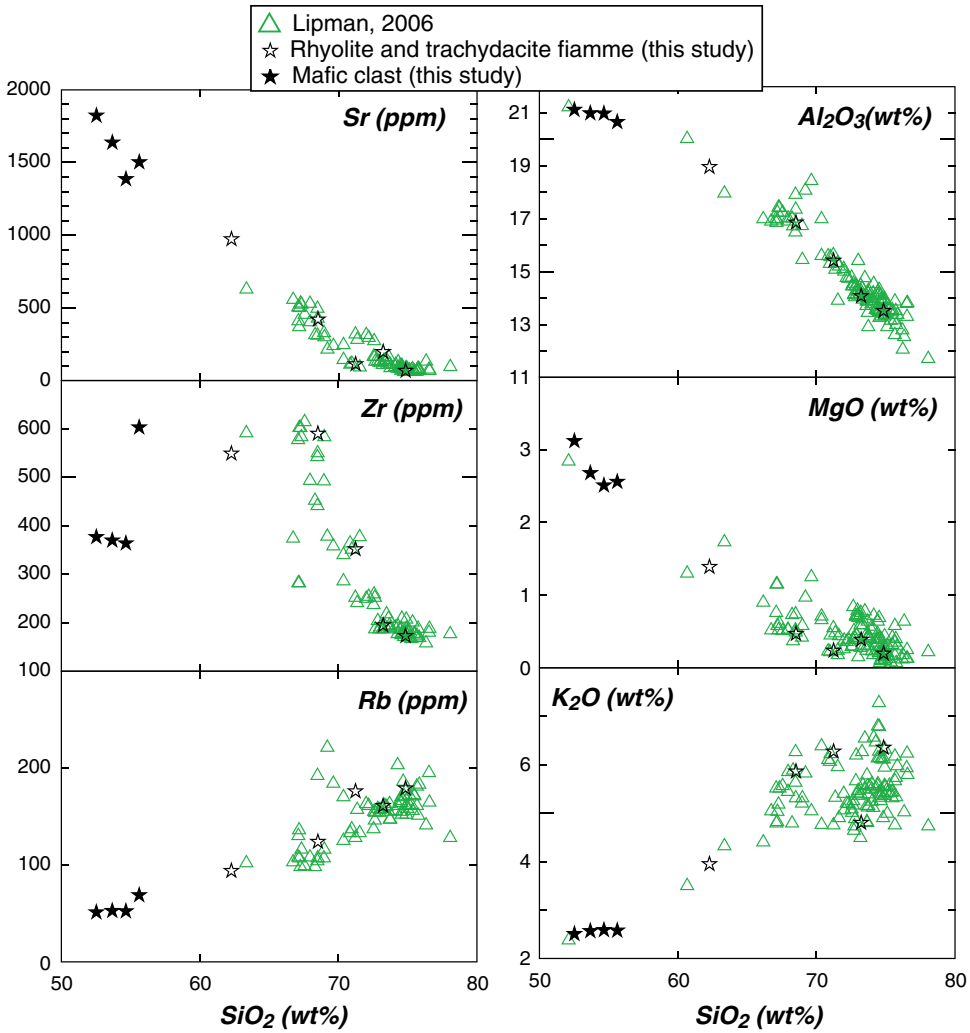

Fig. 1 Major and trace-element whole-rock chemistry of the CRT (data from compiled database, Lipman 2006; and this study). Rocks with >7 wt% K_2O not plotted; these typically have high LOI (Loss On Ignition), and problems of alkali exchange have long been recognized in parts of the CRT, especially ponded intracaldera tuff (Lipman 2000). Some samples were not analyzed for trace elements. Hence, major oxide plots have more data points than trace-element plots

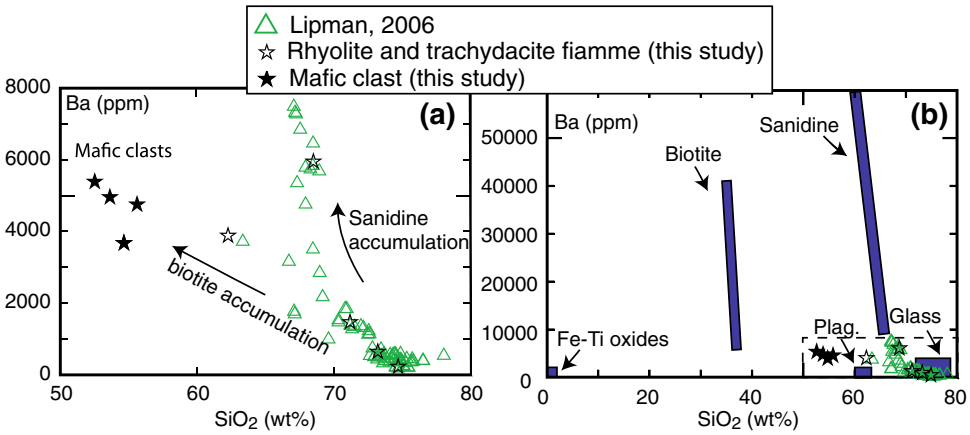

Fig. 2 Ba versus SiO_2 plots for CRT samples. **a** Whole-rock compositions of the different types of samples (Lipman 2006; and this study). **b** Ranges of Ba and SiO_2 concentrations for the major crystal phases in the CRT, which are thought to have generated the mixing trends in **a**

Whole-rock and glass compositions

Whole-rock compositions of the CRT vary strongly from the early erupted, *rhyolitic,* crystal-poor material (~5–10 vol % crystals, 72–76 wt% SiO_2) to late-erupted, *trachydacite*, crystal-rich fiamme (15–40 vol % crystals; <55–69 wt% SiO_2; Whitney 1988; Dorais et al. 1991; Lipman 2006; Figs. 1, 2). Rare, more mafic clasts (52–55 wt% SiO_2) are also present in some locations. Trace elements vary even more strikingly; from rhyolite to

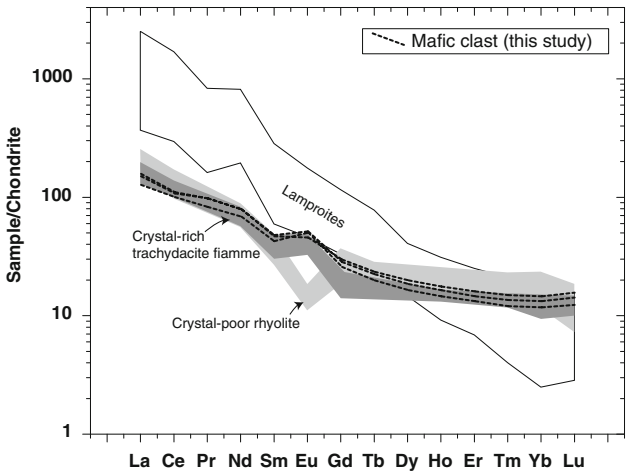

Fig. 3 Chondrite-normalized (McDonough and Sun 1995) rare earth element (REE) concentrations of crystal-poor rhyolite, crystal-rich trachydacite fiamme, and mafic clasts (compiled from Lipman 1975; Lipman 1987; Dorais et al. 1991; Riciputi 1991). Outlined is the field of typical lamproite REE compositions (compiled from Mitchell and Bergman 1991, see also Fig. 19-17 of Winter 2001)

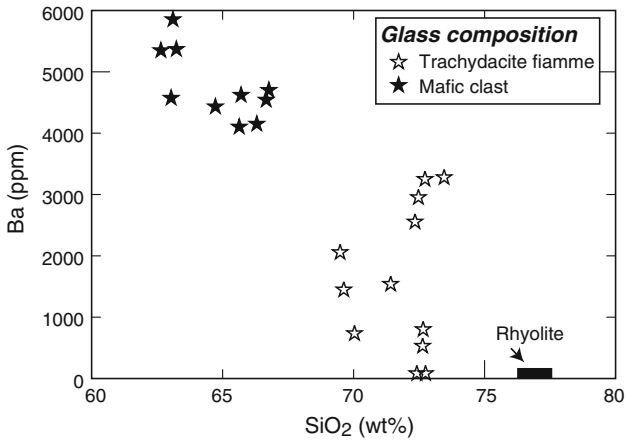

Fig. 4 Glass compositions of CRT juvenile clasts. Some analyses may have suffered K/Na exchange and secondary hydration, but the SiO_2 and Ba concentrations likely are near-magmatic values

trachydacite, Rb decreases nearly twofold (from ~180 to 100 ppm), Zr increases threefold (200–600 ppm), Sr fivefold (100–500 ppm), and Ba nearly 20-fold (300–7,500 ppm; Fig. 2). Trachydacite fiamme and mafic clasts have lower REE concentrations and positive Eu anomalies that are complementary to the negative Eu anomalies observed in the rhyolite (Dorais et al. 1991; Fig. 3).

Glass compositions, obtained by EMPA from crystal-poor rhyolite (Carpenter Ridge locality), crystal-rich fiamme samples (Brown Lake locality), and mafic clasts, also vary significantly in major and trace elements. Glass in crystal-rich fiamme varies from 69 to 74 wt% SiO_2 and from <200 to 3,500 ppm Ba (Fig. 4, Appendix 2 of ESM), while mafic clasts range from 54 to 65 wt% SiO_2 and ~2,600–5,800 ppm Ba. Rhyolitic glass compositions are less variable in major elements (~77–78 wt% SiO_2, 0.03–0.08 wt% MgO) and have low Ba contents (most analyses below detection limit: ~200 ppm).

Mineral assemblage

The crystal-poor rhyolite and crystal-rich trachydacite clasts have the same mineral assemblage, consisting of plagioclase, sanidine, biotite, Fe–Ti oxides, and zircon. Some crystal-rich fiamme contain amphibole and pyroxene. The mafic clasts have a similar assemblage, including abundant amphibole, but lack sanidine (zircon not recognized). Quartz is absent in all samples (as previously noted by Whitney et al. 1988), although the rhyolite is strongly quartz normative (up to 20 %). Crystals in the trachydacite fiamme and mafic clasts are typically large (to several mm), and many of the feldspars and biotite crystals have anhedral outlines and wormy sieve-textured internal cavities (Figs. 5, 6, 7). Groundmass microlites have not been found in any of these samples.

Plagioclase is the dominant phase in all juvenile clasts (~30–50 % of the mineral assemblage, Whitney et al. 1988). It is typically complexly zoned and euhedral in the crystal-poor rhyolite, but commonly anhedral and sieve-textured in the trachydacite fiamme and mafic clasts (Figs. 5, 6). In both the trachydacite and rhyolitic end-members, plagioclase rims have low An contents ($An_{30–20}$), while interiors are highly variable (An_{30-70}, Fig. 8). Some plagioclase crystals in the mafic clasts appear relatively euhedral, with calcic cores (up to An_{85}) and more sodic rims (~An_{50}), while others are more homogeneous, with sodic compositions (as low as An_{38}) and patchy zoning, or strong sieved textures with compositions ~$An_{46–56}$ (Fig. 8). The broad compositional overlap between plagioclase crystals from both trachydacite and rhyolite indicates that they crystallized from a similarly evolved melt. Some plagioclases with low An (~20–30 mol %) in both trachydacite and rhyolite show a trend of increasing Ba, opposite to the mafic trend that leads to the $An_{30–70}$ cores (Fig. 8c).

Sanidine forms both euhedral and highly embayed anhedral crystals (Figs. 5, 6, 7, 8, 9), particularly in the trachydacite clasts (this study; Whitney et al. 1988; Dorais et al. 1991). The crystals are commonly strongly zoned, particularly in Ba, more markedly in the trachydacite fiamme than in the rhyolite (<1–9 wt%, Fig. 9; Whitney et al. 1988; Appendix 2 of ESM). Sanidine crystals can be separated into two main groups: (1) large typically euhedral crystals (>1.5 mm) with low Ba (<~2.5 wt% BaO) and reverse zoning (i.e., high-Ba rims; Fig. 9a, b and (c1))

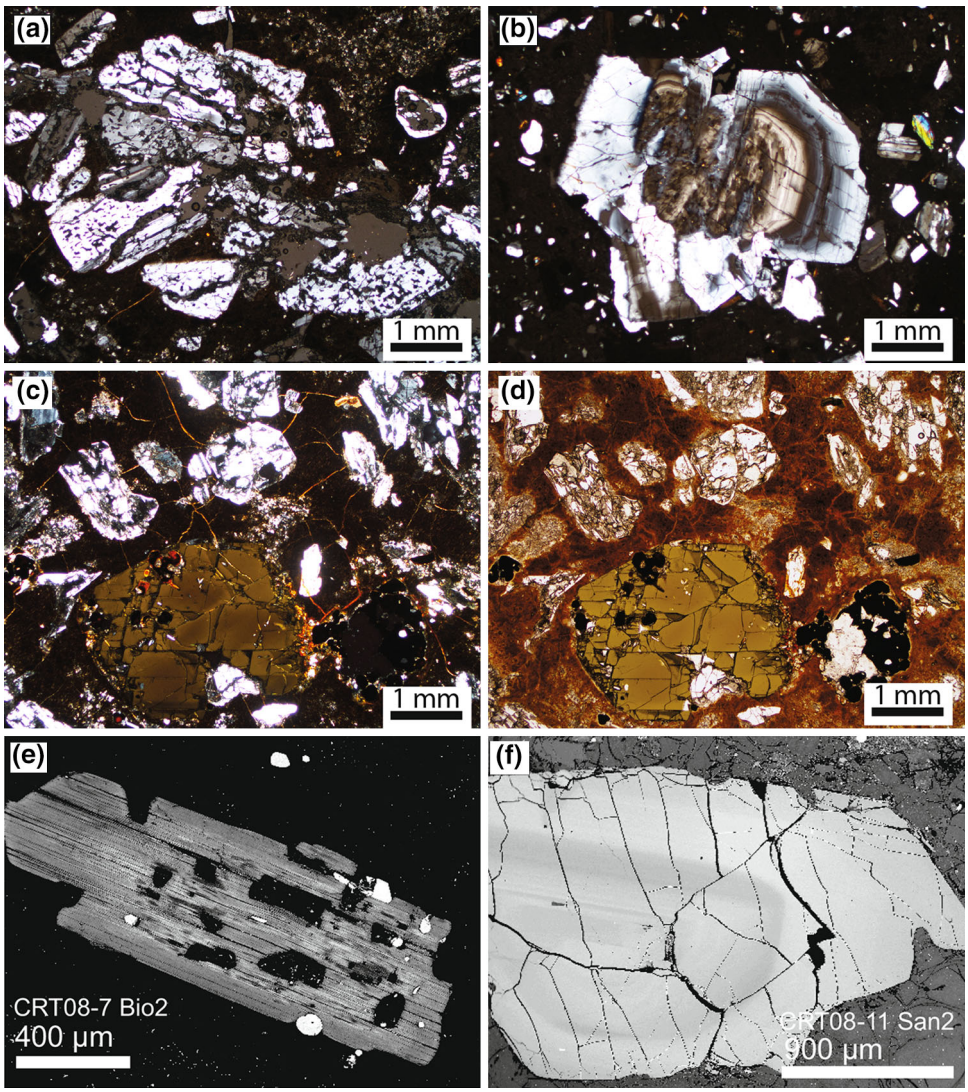

Fig. 5 Textures of crystal-rich trachydacite fiammes (**a**, **b**, CRT08-7 and **c**, **d**, CRT09-2c, photomicrographs). **a** Large anhedral and sieve-textured plagioclase megacryst (aggregation of multiple crystals), suggesting thermal resorption. **b** Large zoned plagioclase crystal with a partly embayed outline. **c** Large crystals of plagioclase, amphibole, and Fe–Ti oxide, in polarized light. **d** Same image, transmitted light. On pictures **c** and **d** plagioclase crystals are typically anhedral and locally sieve-textured, while the large amphibole crystals (*bottom* of image) show no obvious signs of disequilibrium. **e** Backscatter electron image of anhedral and embayed biotite with internal cavities, sample CRT08-7. **f** Backscatter electron image of sanidine showing dark low Ba anhedral core overgrown by higher-Ba rim that is also anhedral, sample CRT08-11

and (2) smaller crystals (typically <1 mm, both euhedral and embayed) that have moderate to high Ba (~1.5 to ~9 wt% BaO) and are both normally and reversely zoned (Fig. 9(c3)).

Ferromagnesian phases are dominantly biotite and amphibole (±rare pyroxene, not analyzed in this study: see Dorais et al. 1991). Biotite makes up to a few percent of the modal assemblage in both the fiamme and clasts. Crystals can be both euhedral and strongly anhedral/wormy (Fig. 7). Like sanidine, biotite crystals are notably zoned in Ba (Whitney et al. 1988; Dorais et al. 1991; Appendix 2 of ESM, Fig. 7). BaO contents vary from below the detection limit (mostly in cores) to above 4 wt%. (to 4.8–5 wt% in clasts). Most amphibole phenocrysts in the CRT have Na, K, Ti, and Al concentrations that are higher than the main amphibole population of the Fish Canyon Tuff (Figs. 8 and 10, Appendix 2 of ESM; Dorais et al. 1991; Bachmann and Dungan 2002), although a few data points from Riciputi (1991) suggest that low-Al amphiboles are also sparsely present in the intracaldera trachydacite CRT (Mammoth Mountain Member, Fig. 10). Amphiboles in clasts are similar to those in the trachydacite fiamme, with Al_2O_3 content about 11–12 wt% (Figs. 7 and 10).

Both magnetite and ilmenite are minor, albeit ubiquitous, phases. Magnetite has a wide compositional range (X_{Usp} of 0.2– >0.5), with Ti contents in the trachydacite fiamme typically higher than those in the rhyolite (Whitney et al. 1988). In contrast, ilmenite compositions are less variable in both rhyolitic and trachydacite clasts (X_{Ilm} from 0.86 to 0.91; Whitney et al. 1988).

Pre-eruptive reservoir conditions

Fe–Ti oxide thermometry in CRT samples shows a wide range of pre-eruptive temperatures (Ilm–Mag equilibrium

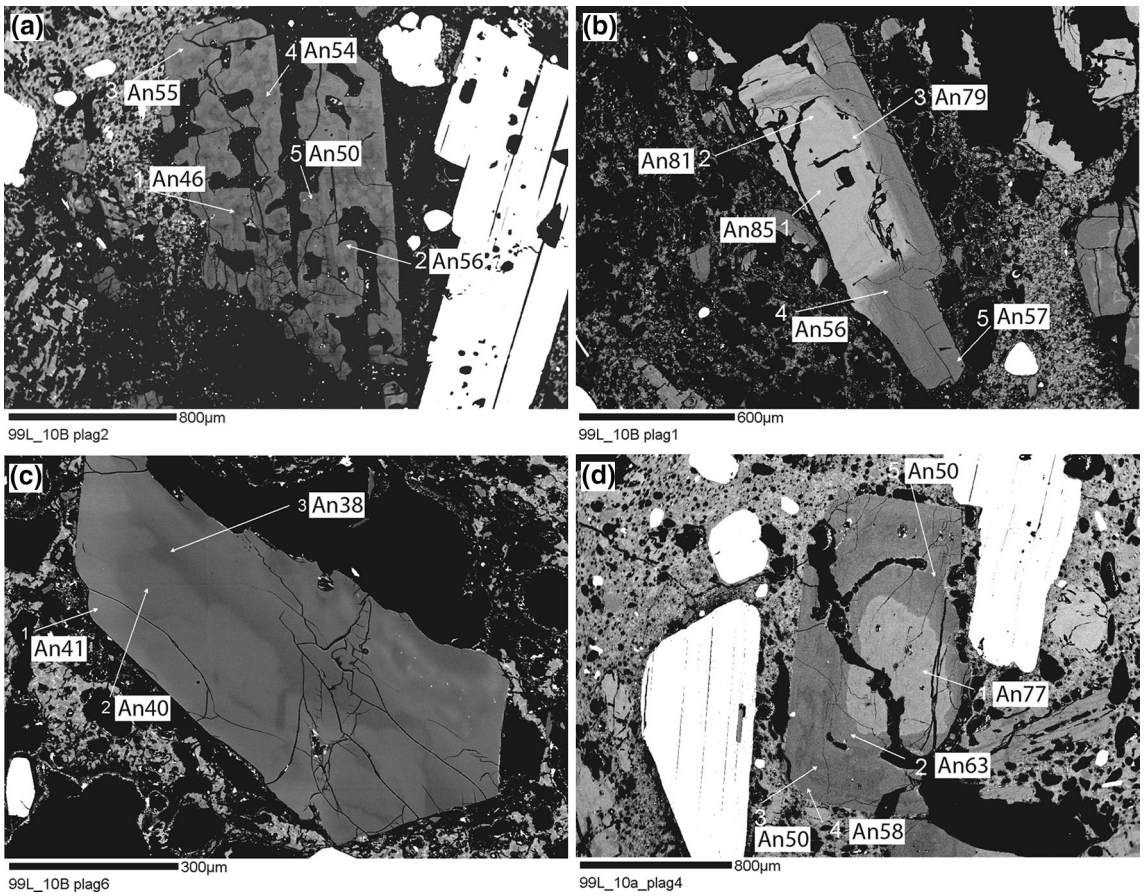

Fig. 6 Plagioclase textures and An content from mafic clasts, showing variability among crystals within single thin sections. In section 99L-10B, adjacent plagioclase crystals show **a** highly anhedral, sieve texture at relatively uniform composition, **b** near-euhedral calcic core, truncated by uniform sodic overgrowth (fractures and the rectilinear hole in the core likely due to polishing), and **c** absence of significant compositional zoning or sieve resorption. **d** Anhedral calcic core surrounded by oscillatory zoned rim area, section 99L-10A

pairs from Whitney et al. 1988, no new data from this study). In the rhyolite, the temperatures vary from ~750 to 810 °C, while in the trachydacite fiamme, the range is ~850–1,000 °C (Whitney et al. 1988). Pressure of crystallization was estimated at 100–200 MPa for the rhyolitic samples on the basis of experimental phase equilibria (particularly, absence of quartz in this quartz-normative magma; Whitney et al. 1988; Gualda et al. 2012). Newly determined amphibole compositions from the trachydacite fiamme and mafic clasts (Appendix 2 of ESM) yield temperatures of 930 to 990 ± 25 °C (formulation of Ridolfi et al. 2010), higher than from most coexisting Fe–Ti oxides. Similarly, amphibole barometry (Ridolfi et al. 2010) yields pressures from 280 to 370 ± 100 MPa for both clasts and fiamme, indicating 10–14 km depth (assuming an average density of 2,800 kg/m^3 for the crust), suggesting that most hornblende crystals grew at higher temperature and/or slightly greater depths than the rest of the mineral assemblage.

Discussion

Origin of the trachydacite fiamme and mafic clasts

Dorais et al. (1991) suggested that the trachydacite fiamme were derived from alkaline magma that mixed with a melt-rich rhyolite on the basis of: (1) the high Na + K, Ba, and Zr content of the bulk material, (2) the high Ba content in sanidine and biotite, and (3) the high alkali and Ti contents in amphibole. As evidence for mixing, they cited: (1) "plastically deformed" fiamme, (2) disaggregation of fiamme and crystal exchange, and (3) a thermal gradient based on higher temperatures deduced for the trachydacite magma (Whitney et al. 1988; Dorais et al. 1991). While the evidence cited above is consistent with mixing between two magmas of contrasting thermal, physical, and geochemical properties, some of the observed textures could have formed by decompression-induced growth during magma ascent prior to eruption, as shown by recent

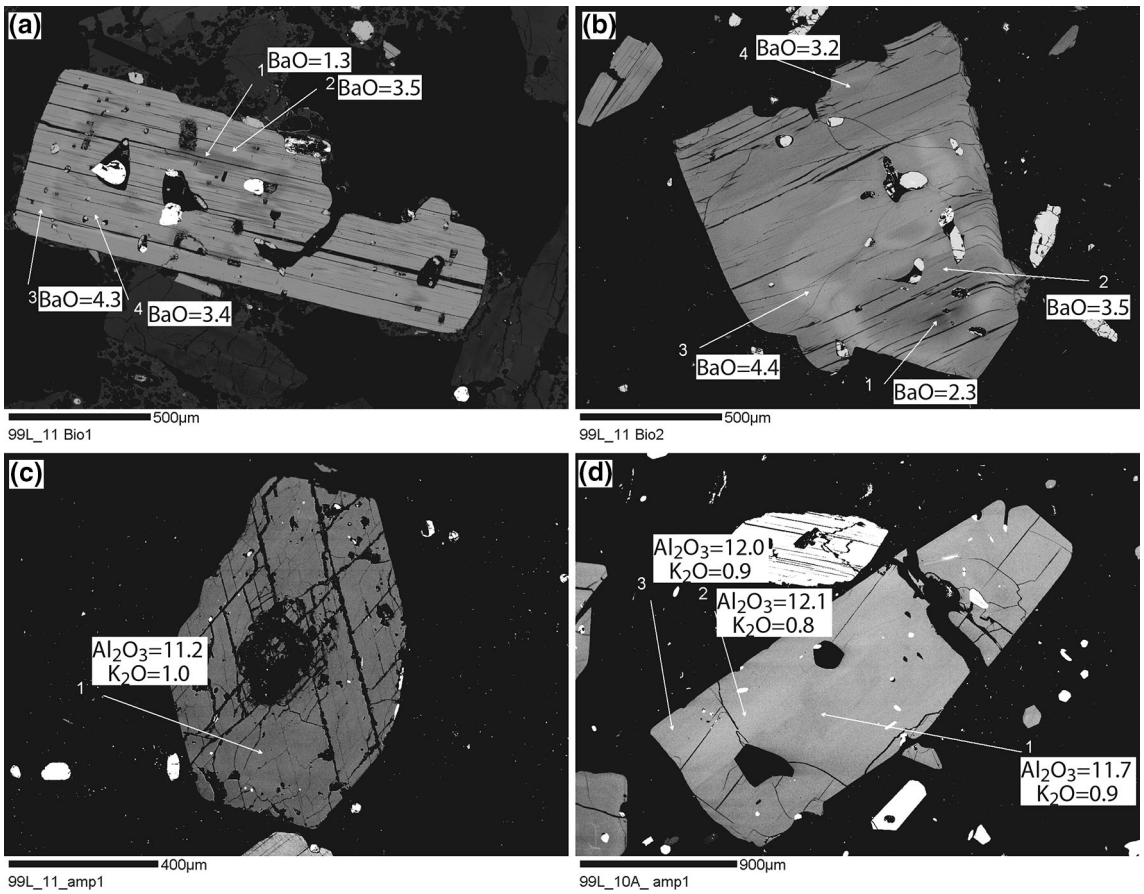

Fig. 7 Biotite and amphibole textures and composition from the mafic clasts (99L-11, 99L-10A). **a**, **b** Biotite crystals show reverse zoning in Ba and rounded outlines. **c**, **d** Amphiboles appear more euhedral and have relatively high Al_2O_3, but low K_2O contents

experiments (e.g., Hammer 2006; Crabtree and Lange 2011). However, the large size of most CRT crystals (Figs. 5, 6) and the absence of microlites are inconsistent with growth as the dominant process generating these complex textures (although it may have produced some of the final crystal outlines). In light of the observations listed above, we agree with Dorais et al. (1991) that temperature-induced dissolution was the main mechanism leading to the anhedral and embayed shapes of the crystals (when not overgrown by a new rim).

Although the textural evidence of mixing is undeniable, several observations contradict the inference that the fiamme and mafic clasts are of a *strongly* alkaline parentage. First, whole-rock compositions of the fiamme plot in the subalkaline field (highly quartz normative, with $Na_2O + K_2O$ <11 wt%), in keeping with all other magmas that have erupted in the SRMVF. Second, REE patterns do not display the steep, LREE-enriched signature that is typical of alkaline magmas (Fig. 3), but show a clear positive Eu anomaly. Third, the FeO_{tot}/MgO ratios of biotite in the CRT (0.6–1.7) are far lower than those from alkaline suites (average of ~3.5 for biotite from peraluminous magmas, ~7 for biotite in anorogenic alkalic suites) and close to the 1.76 average for biotite in calc-alkaline series (Abdel-Rahman 1994). Finally, the trachydacite fiamme reach bulk-rock Ba concentrations (4,000–7,500 ppm) that are higher than the most Ba-enriched alkaline magmas (e.g., lamproites, Mitchell and Bergman 1991). The majority of alkaline volcanic rocks are lower than 2,500–3,000 ppm Ba (e.g., Pe-Piper and Piper 2002; Wiesmaier et al. 2012). Hence, these clasts are unlikely to represent any *'liquid'* magma composition. As already pointed out by Dorais et al. (1991), we stress the lack of linear mixing trends in bulk-rock variation diagrams (our Figs. 1 and 2; Fig. 6 of Dorais et al. 1991), indicating that a simple binary mixing model cannot fully explain the textural and compositional variability in the CRT.

An alternative explanation for the high Na + K, Ba, Sr, and Zr concentrations is that the late-erupted fiamme and mafic clasts represent deeper parts of the magma reservoir that had accumulated feldspars, biotite and zircon (silicic cumulate)—a model considered by Dorais et al. (1991), but rejected on the basis of the above-mentioned high Ba content of whole-rock and phenocrysts. However, high Ba

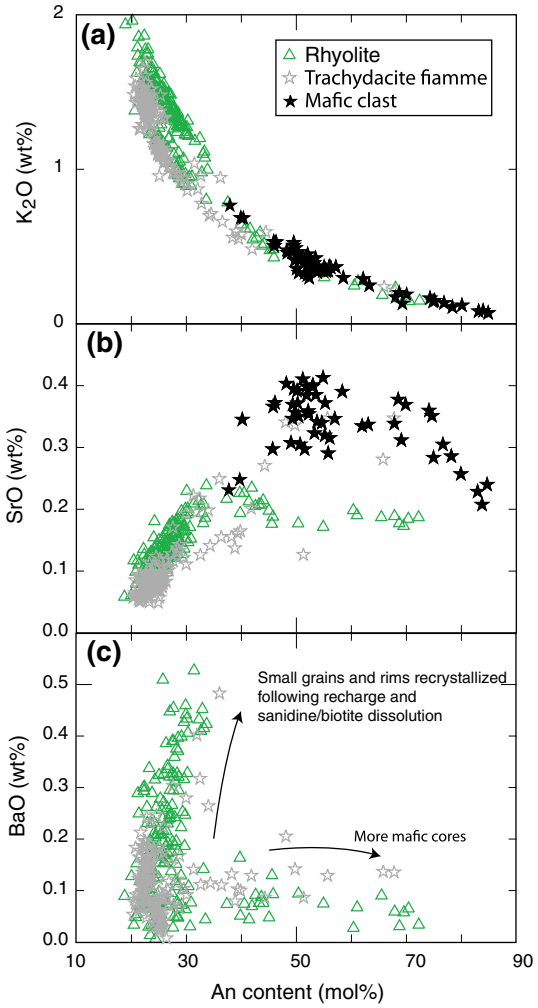

Fig. 8 Plagioclase compositions from the mafic clasts, crystal-rich trachydacite fiamme and crystal-poor rhyolite in the CRT. **a** K_2O versus An content, **b** K_2O versus An content, and **c** BaO versus An content (BaO was not analyzed in plagioclase crystals from clasts due to their low concentrations). Note the two trends in BaO–An space in **c**

in both whole rock and phenocrysts is consistent with assimilation of a feldspar- and biotite-rich cumulate (Fig. 2) that *partially melted* after a hot recharge event, followed by partial recrystallization of some phases (sanidine, biotite, and plagioclase) from a trace-element-enriched interstitial melt (leading to the different trends seen in plagioclase compositions, Fig. 8c). The high Zr/Hf ratios (~49) in the mafic clasts are also compatible with some zircon accumulation in these samples (see Deering and Bachmann 2010). The incorporation of around 20 % sanidine and/or biotite is sufficient to raise the rock composition from ~1,000–1,500 ppm to 6,000–8,000 pm (assuming an average of 25,000–40,000 ppm Ba in biotite and sanidine; see modeling discussion below). As trace-element contents are much more sensitive to contamination than major elements (Fig. 1 of Appendix 3 of ESM), the relatively low K contents of the mafic clasts are expected (mixing 20 % of biotite or sanidine with ~7–9 wt% K_2O with 80 % of low-K magma produces the observed 2.5 wt% K_2O in the bulk rock).

The high Ba concentrations in some CRT biotite (to 45,000 ppm) and sanidine (to 70,000 ppm) yield melt Ba concentrations on the order of 3,500 ppm, using the highest possible partition coefficient (~20; e.g., Nash and Crecraft 1985), which is similar to the highest Ba measured in the CRT glass. Lower partition coefficients would yield even higher Ba contents in the melt. As such concentrations are rare in erupted rocks and unknown for high-SiO_2 rhyolite, we suggest that *local enrichment* of Ba around melting sanidine and biotite is the only mechanism that can account for the extreme concentrations. Notably, (1) Ba concentrations are highest in the smallest sanidine crystals (<500 um), while larger grains (>1 mm) have lower concentrations in their cores (some <5,000 ppm, similar to other San Juan units, such as the Fish Canyon Tuff, see Bachmann et al. 2005), and (2) commonly are reversely zoned (high-Ba rims; Fig. 7 and 9). The presence of biotite and plagioclase crystals with high-Ba rims also supports localized, high-Ba, environments in which biotite crystals grew. Heterogeneous Ba concentrations are likely to persist, as Ba diffuses particularly slowly in silicate melts (Zhang and Cherniak 2010).

The trachydacite zone high in the thick intracaldera CRT accumulation (Mammoth Mountain Member, 66–68 % SiO_2) is interpreted as a portion of the cumulate with a slightly different composition/modal proportion than the trachydacite fiamme in the outflow facies. As discussed previously, mineral proportions and compositions of this Mammoth Mountain Member appear to be broadly similar to those in the crystal-poor rhyolite, e.g., subequal modal sanidine and plagioclase with similar compositions to those found in the rhyolite (Dorais et al. 1991; Riciputi 1991); presence of clinopyroxene; and lower Al (lower pressure?) amphibole compositions (Fig. 10). The chemical and mineralogical variability of the inferred cumulate fragments (trachydacite fiamme in outflow and intracaldera facies, mafic clasts) suggests that modal mineralogy can be rather variable in the leftover crystal residue. Such mineralogical complexities are documented in some plutons with cumulate zones (e.g., Bachl et al. 2001; Turnbull et al. 2010).

Trace-element modeling can test further the potential link between trachydacite fiamme and rhyolitic compositions as, respectively, end-members of the leftover cumulate and the complementary extracted melt of a differentiating magma reservoir with an initial dacitic composition between these two end-members (Fig. 11; see Mohamed 1998; Deering et al. 2011b, for similar modeling

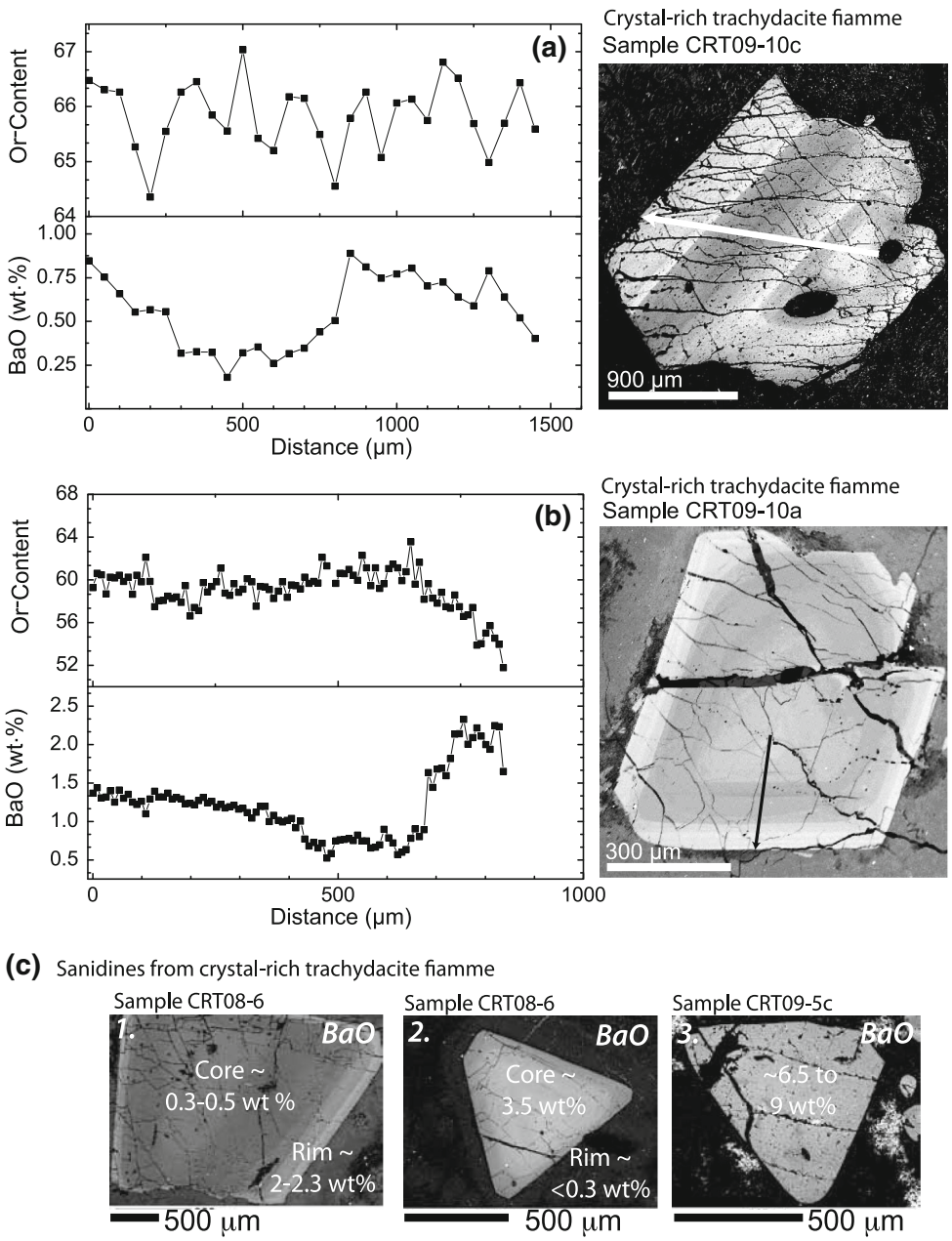

Fig. 9 Backscatter electron images of sanidine and EMP data from crystal-rich trachydacite fiamme. **a**, **b** Show BaO and orthoclase (Or) concentration profiles from interior to rim (*line* with *arrow*). Many large phenocrysts from both crystal-rich and crystal-poor material typically have low BaO cores (<1 wt%)

exercises), keeping in mind that mixing/mingling with recharge magma will also impact compositions of the erupted material. The Ba, Sr, and Rb contents of an extracted melt and resulting residua are modeled using simple Rayleigh fractionation equations for both the liquid and residual cumulate (Appendix 3 of ESM, Tables 2, 3; Shaw 1970; Rollinson 1993; using equilibrium fractionation here is not justified given the slow diffusion rates for these elements and would not change the main trend). Modal proportions for the models are set to match the observed mineral assemblage of the fiamme. Initial trace-element concentrations were determined graphically using Harker diagrams (e.g., a composition between the fiamme and rhyolite: star symbol in Fig. 11; Appendix 3 of ESM, Table 2).

This model generates appropriate trace-element concentrations of Ba, Sr, and Rb for the end-members across a range of melt fractions (F), resulting, at the extremes, in a cumulate with high Ba–Sr (the trachydacite fiamme), and a melt-rich component (e.g., rhyolite) with low Ba–Sr, using widely accepted distribution coefficients (Nash and Crecraft 1985; Rollinson 1993; Appendix 3 of ESM, Table 3) and reasonable initial concentrations for these elements. In addition, the Zr distribution can be produced by the crystallization and accumulation of ~0.06 modal percent zircon without discernible impact on the evolution of Ba, Sr,

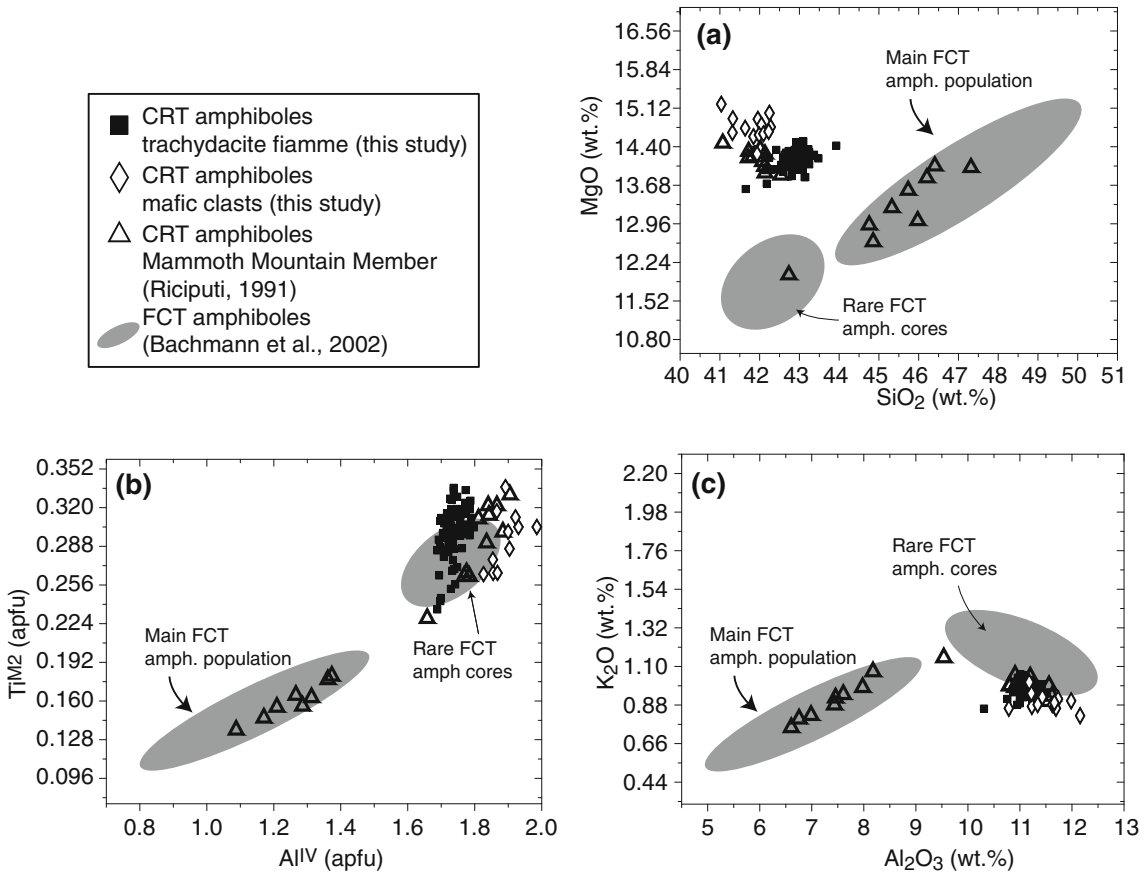

Fig. 10 Representative CRT amphibole compositions (this study; Riciputi 1991), compared to Fish Canyon Tuff (FCT, *gray shaded fields*; Bachmann et al. 2002). The low Al, Ti compositions for the CRT, which plot with the main FCT population, are from the Mammoth Mountain Member (data from Riciputi 1991). The high-Al, Ti compositions from the FCT are rare pargasitic cores, interpreted as relicts from deeper, hotter conditions of crystallization

or Rb. Compared with the rhyolite, similar to slightly depleted LREE patterns and positive Eu anomalies in the fiamme and mafic clasts (Fig. 3) are consistent with the entrainment of plagioclase-rich cumulate (see Deering et al. 2011b for a similar modeling exercise). Differing amount of melt extraction, variable crystallization conditions (e.g., depth and temperature of crystallization), and mixing/mingling with more mafic recharge would also have participated in producing the geochemical complexity of the non-rhyolitic parts of the erupted material.

A key aspect of the controversy surrounding the origin of zoned ignimbrites is the tendency to apply only one of the end-member models discussed above (magma mixing following recharge of either mafic or silicic magmas versus in situ differentiation with crystal–liquid separation leading to chemical heterogeneities). Clearly, the CRT has elements of both. Late recharge and associated reheating–remelting of an already chemically zoned chamber (by in situ differentiation) seems necessary to reconcile the following observations: (1) the thermal gradient indicated by the Fe–Ti oxides, (2) the relatively low crystal content of the trachydacite fiamme (mostly <35 vol %) relative to the crystal fraction required by fractionation models, (3) the geochemical variability of the non-rhyolitic CRT deposit (including mafic clasts), (4) the high Ba–Sr content of the melt, (5) the embayed sieved textures and common reverse zoning patterns in both biotite and sanidine, and (6) the presence of moderately high-pressure, high-temperature amphiboles in the trachydacite fiamme. Evidence for pre-eruptive recharge is ubiquitous in incrementally built magma reservoirs (e.g., Lipman 2007) and should be expected in the CRT. Some partial melting of the crystalline material is required for the cumulate, which likely reached >75 vol % crystals, to erupt (Deering et al. 2011b).

Conclusions

We propose the following model to explain the chemically and thermally zoned 1,000 km^3 CRT, building upon previous studies of similar units (e.g., Lipman 1967; Hildreth 1981; Worner and Schmincke 1984a; Worner et al. 1985;

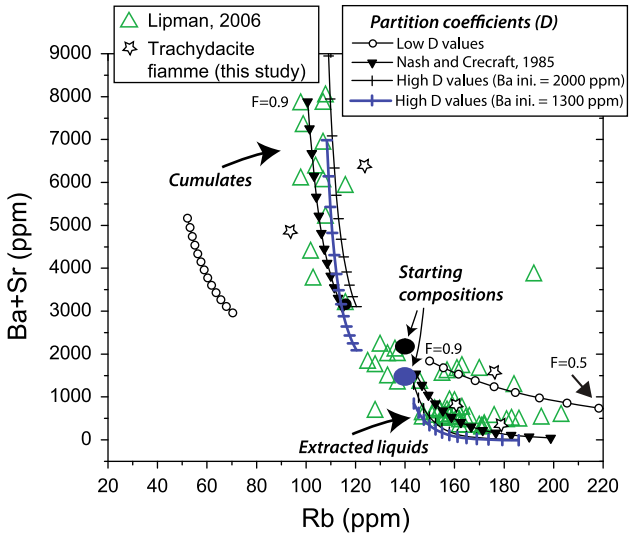

Fig. 11 Trace-element modeling using Rb, Ba, and Sr. Tick marks are melt fraction increments of 0.05, ranging from $F = 0.9$–0.3, except where marked. *Ellipses* denote starting compositions. Mineral proportions for determining the bulk partition coefficients are based on the crystal-rich fiamme, using a range of distribution coefficients (e.g., high/low Ds) from Rollinson (1993) and an intermediate set from Nash and Crecraft (1985). CRT compositions (*triangle symbols*) are plotted for comparison (compilation from Lipman 2006; this study)

Bacon and Druitt 1988; Grunder and Mahood 1988; Hildreth and Fierstein 2000; Hildreth 2004; Fowler and Spera 2010; Evans and Bachmann 2013; Pamukcu et al. 2013). After the eruption of the massive Fish Canyon Tuff at ~28 Ma, an upper-crustal magma reservoir regrew in the same area by incremental addition of similar high-K calc-alkaline dacite that has formed the Fish Canyon Tuff. This magma reservoir was dominantly maintained in a mush state (Marsh 1981; Koyaguchi and Kaneko 1999; Huber et al. 2009) as it grew in a pre-warmed upper crust, undergoing differentiation by crystal–liquid separation at intermediate (50–70 vol %) crystallinity (Brophy 1991; Bachmann and Bergantz 2004; Dufek and Bachmann 2010), and resulting in a liquid-rich cap with its residual cumulate. Reheating and partial resorption of low-temperature phases (e.g., feldspars and biotite) toward the top of the cumulate, due to recharge shortly prior to eruption, reduced crystallinity and allowed scouring of the top of the cumulate mush at the end of the eruption: The observed range of ~5–35 vol % crystals is much lower than the expected crystallinity of ~65–80 % at the time of melt extraction (e.g., Deering et al. 2011a, b). Such a late recharge is recorded in the CRT by the presence of amphibole and Fe–Ti oxide that reveal P–T gradients. Resorption of low-temperature mineral phases (sanidine, biotite, and some low-An plagioclase) caused by this reheating accounts for observed textural complexities and local enrichments in Ba and Sr in the melt, while high-Ba rims on large sanidine and biotite phenocrysts require late crystallization from this enriched melt following resorption. Entrainment of minor phases from the cumulate, such as zircon, explains the other unusual concentrations in trace elements in the trachydacite fiamme.

The CRT shares a number of features with many other zoned ignimbrites observed globally (thermal, compositional, and crystallinity gradients), regardless of tectonic setting or mode of origin (calc-alkaline, alkaline, and peralkaline). However, explanations for the origin of the full spectrum of erupted compositions vary considerably (e.g., Bacon and Druitt 1988; Wolff et al. 1990; Civetta et al. 1997; Brown et al. 1998; de Silva et al. 2001; Troll and Schmincke 2002; Ginibre et al. 2004; Hildreth and Wilson 2007). Although many have suggested that the crystal-rich and crystal-poor portions of the reservoir were related by fractional crystallization, the crystal-rich portion is not always recognized as a remobilized cumulate (i.e., a crystalline portion of the reservoir that has physically accumulated crystals). Rather, the zoning is more commonly interpreted as the result of fractionating from a slightly less-evolved portion of the magma reservoir or a simple binary mixing between two different magmas. Recent studies (i.e., the Ammonia Tanks Tuff, Deering et al. 2011b; the Peach Spring Tuff, Pamukcu et al. 2013; and the Bishop Tuff, Evans and Bachmann 2013), in addition to this one, have indicated that late-erupted material from several of the largest compositionally zoned ignimbrites in North America includes crystal-rich cumulates from the upper-crustal reservoir, exhumed by heating, dissolution, and remobilization during eruption. These observations require that the processes important in forming these zoned ignimbrites, and, in particular, the rhyolitic melt pockets, occur at relatively shallow depths (5–10 km depth in most regions) and include both mixing and fractionation—neither in isolation. In fact, mixing/recharge is likely a necessary process required to remobilize any part of these cumulate piles, assuming that high crystallinities (>70 vol % crystals) must be achieved in these zones to produce the melt-rich rhyolite caps. It is also expected that most of the cumulate zone, which was not partially molten prior to eruption, remained in the ground as plutonic leftovers. Therefore, a growing body of evidence now indicates that in situ crystal–liquid separation into a lower crystal-rich cumulate zone, and upper eruptible lenses, is common in incrementally built upper-crustal magma reservoirs of high-flux magmatic provinces.

Acknowledgments We thank Mike Dungan and Christian Huber for their many years of support, both in the logistic and the scientific aspects of this project. The Volcanology and Petrology Group at the University of Washington is thanked for their support and for creating a fertile research environment. We also thank Dr. Scott Kuehner

(University of Washington) for his superb analytical expertise and assistance. Thoughtful reviews by R. Lange, C. Wilson, A. Grunder, and two anonymous reviewers substantially improved the final manuscript. This work was partly supported by fellowships received by C. Plummer from the GO-MAP program (University of Washington), ARCS–Seattle Chapter, and the National Science Foundation [DGE-0718124]. Field work and analytical work were funded by the US National Science Foundation [EAR 0809828] and Swiss National Science Foundation (grant # 200021_146268) to Bachmann.

References

Abdel-Rahman AFM (1994) Nature of biotites from alkaline, calc-alkaline, and peraluminous magmas. J Petrol 35:525–541

Bachl CA, Miller CF, Miller JS, Faulds JE (2001) Construction of a pluton: evidence from an exposed cross-section of the Searchlight pluton, Eldorado Mountains, Nevada. Geol Soc Am Bull 113:1213–1228

Bachmann O, Bergantz GW (2004) On the origin of crystal-poor rhyolites: extracted from batholithic crystal mushes. J Petrol 45:1565–1582

Bachmann O, Dungan MA (2002) Temperature-induced Al-zoning in hornblendes of the Fish Canyon magma, Colorado. Am Mineral 87:1062–1076

Bachmann O, Dungan MA, Lipman PW (2002) The Fish Canyon magma body, San Juan volcanic field, Colorado: rejuvenation and eruption of an upper-crustal batholith. J Petrol 43(8):1469–1503

Bachmann O, Dungan MA, Bussy F (2005) Insights into shallow magmatic processes in large silicic magma bodies: the trace element record in the Fish Canyon magma body, Colorado. Contrib Miner Petrol 149:338–349

Bacon CR, Druitt TH (1988) Compositional evolution of the zoned calc-alkaline magma chamber of Mount Mazama, Crater Lake, Oregon. Contrib Miner Petrol 98:224–256

Brophy JG (1991) Composition gaps, critical crystallinity, and fractional crystallization in orogenic (calc-alkaline) magmatic systems. Contrib Miner Petrol 109(2):173–182

Brown SJA, Wilson CJN, Cole JW, Wooden JL (1998) The Whakamaru Group ignimbrites, Taupo volcanic zone, New Zealand; evidence for reverse tapping of a zoned silicic magmatic system. J Volcanol Geoth Res 84(1–2):1–37

Civetta L, Orsi G, Pappalardo L, Fisher RV, Heiken G, Ort M (1997) Geochemical zoning, mingling, eruptive dynamics and depositional processes-the Campanian Ignimbrite, Campi Flegrei, Italy. J Volcanol Geoth Res 75:183–219

Crabtree SM, Lange RA (2011) Complex Phenocryst Textures and Zoning Patterns in Andesites and Dacites: evidence of Degassing-Induced Rapid Crystallization? J Petrol 52(1):3–38

de Silva S, Eichelberger JC, Chertkoff DG, Dreher ST, Nye CJ (2001) Magmas in collision; rethinking chemical zonation in silicic magmas; discussion and reply [modified]. Geology 29(11):1063–1064

Deering CD, Bachmann O (2010) Trace element indicators of crystal accumulation in silicic igneous rocks. Earth and Planetary Science Letters 297(1–2):324–331

Deering CD, Bachmann O, Dufek J, Gravley DM (2011a) Rift-Related Transition From Andesite to Rhyolite Volcanism in the Taupo Volcanic Zone (New Zealand) controlled by Crystal-Melt Dynamics in Mush Zones With Variable Mineral Assemblages. J Petrol 52(11):2243–2263

Deering CD, Bachmann O, Vogel TA (2011b) The Ammonia Tanks Tuff: erupting a melt-rich rhyolite cap and its remobilized crystal cumulate. Earth and Planetary Science Letters 310(3–4): 518–525

Dorais MJ, Whitney JA, Stormer JC (1991) Mineralogical constraints on the petrogenesis of trachytic inclusions, Carpenter Ridge Tuff, Central San Juan volcanic field. Colorado. Contributions to Mineralogy and Petrology 107(2):219–230

Dufek J, Bachmann O (2010) Quantum magmatism: magmatic compositional gaps generated by melt-crystal dynamics. Geology 38:687–690

Dunbar NW, Kyle PR, Wilson CJN (1989) Evidence for limited zonation in silicic magma systems, Taupo volcanic zone. New Zealand. Geology 17(3):234–236

Eichelberger JC, Chertkoff DG, Dreher ST, Nye CJ (2000) Magmas in collision; rethinking chemical zonation in silicic magmas. Geology 28(7):603–606

Ellis BS, Wolff JA (2012) Complex storage of rhyolite in the central Snake River Plain. J Volcanol Geoth Res 211–212:1–11

Evans BW, Bachmann O (2013) Implications of equilibrium and disequilibrium among crystal phases in the Bishop Tuff. Am Mineral 98:271–274

Folkes CB, de Silva SL, Wright HM, Cas RAF (2011) Geochemical homogeneity of a long-lived, large silicic system; evidence from the Cerro Galán caldera, NW Argentina. Bulletin of Volcanology

Fowler SJ, Spera FJ (2010) A Metamodel for Crustal Magmatism: phase Equilibria of Giant Ignimbrites. J Petrol 51(9):1783–1830

Ginibre C, Worner G, Kronz A (2004) Structure and dynamics of the Laacher See Magma Chamber (Eifel, Germany) from major and trace element Zoning in Sanidine: a cathodoluminescence and electron microprobe study. J Petrology 45(11):2197–2223

Grunder AL, Mahood GA (1988) Physical and chemical models of zoned silicic magmas: the Loma Seca Tuff and Calabozos caldera, southern Andes. J Petrol 29(4):831–867

Gualda GAR, Ghiorso MS, Lemons RV, Carly TL (2012) Rhyolite-MELTS: A modified calibration of MELTS optimized for silica-rich, fluid-bearing magmatic systems. Journal of Petrology

Hammer JE (2006) Influence of fO2 and cooling rate on the kinetics and energetics of Fe-rich basalt crystallization. Earth and Planetary Science Letters 248(3–4):618–637

Hildreth W (1979) The Bishop Tuff: evidence for the origin of the compositional zonation in silicic magma chambers. In: Chapin CE, Elston WE (eds) Ash-Flow Tuffs, vol 180. Geological Society of America, Special Paper, pp 43–76

Hildreth W (1981) Gradients in silicic magma chambers: implications for lithospheric magmatism. J Geophys Res 86(B11): 10153–10192

Hildreth WS (2004) Volcanological perspectives on Long Valley, Mammoth Mountain, and Mono Craters: several contiguous but discrete systems. J Volcanol Geoth Res 136(3–4):169–198

Hildreth W, Fierstein J (2000) Katmai volcanic cluster and the great eruption of 1912. Geol Soc Am Bull 112(10):1594–1620

Hildreth WS, Wilson CJN (2007) Compositional Zoning in the Bishop Tuff. J Petrol 48(5):951–999

Huber C, Bachmann O, Manga M (2009) Homogenization processes in silicic magma chambers by stirring and latent heat buffering. Earth and Planetary Science Letters 283:38–47

Koyaguchi T, Kaneko K (1999) A two-stage thermal evolution model of magmas in continental crust. J Petrol 40(2):241–254

Lindsay JM, Schmitt AK, Trumbull RB, De Silva SL, Siebel W, Emmermann R (2001) Magmatic evolution of the La Pacana caldera system, Central Andes, Chile: compositional variation of two cogenetic, large-volume felsic ignimbrites. J Petrol 42(3):459–486

Lipman PW (1967) Mineral and chemical variations within an ash-flow sheet from Aso caldera, South Western Japan. Contrib Miner Petrol 16:300–327

Lipman PW (1975) Evolution of the Platoro caldera complex and related volcanic rocks, southeastern San Juan mountains, Colorado. US Geological Survey Professional Paper 852:128 p

Lipman PW (1987) Rare-earth-element compositions of Cenozoic volcanic rocks in the Southern Rocky Mountains and adjacent areas. US Geological Survey Bulletin 1668, p 23

Lipman PW (2000) The central San Juan caldera cluster: regional volcanic framework. In: Bethke PM, Hay RL (eds) Ancient Lake Creede: its volcano-tectonic setting, history of sedimentation, and relation of mineralization in the creede mining district. Geological Society of America Special Paper 346, pp 9–69

Lipman PW (2006) Chemical Analyses Of Tertiary Volcanic Rocks, Central San Juan Caldera Complex, Southwestern Colorado, Open-File Report 2004-1194

Lipman PW (2007) Incremental assembly and prolonged consolidation of Cordilleran magma chambers: evidence from the Southern Rocky Mountain volcanic field. Geosphere 3(1):1–29

Lipman PW, McIntosh WC (2008) Eruptive and noneruptive calderas, northeastern San Juan Mountains, Colorado: where did the ignimbrites come from? Geol Soc Am Bull 120(7–8):771–795

Lipman PW, Christiansen RL, O'Connor JT (1966) A compositionally zoned ash-flow sheet in southern Nevada. US Geological Survey Professional Paper 524-F:1-47

Lipman PW, Doe B, Hedge C (1978) Petrologic evolution of the San Juan volcanic field, Southwestern Colorado: Pb and Sr isotope evidence. Geol Soc Am Bull 89:59–82

Marsh BD (1981) On the crystallinity, probability of occurrence, and rheology of lava and magma. Contrib Miner Petrol 78:85–98

McDonough WF, Sun S-s (1995) The composition of the Earth. Chemical Geology 120:223–253

Mitchell RH, Bergman SC (1991) The petrology of lamproites. Plenum Press, New York

Mohamed FH (1998) Geochemistry and petrogenesis of El Gezira ring complex, Egypt: a monzosyenite cumulate derived from fractional crystallization of trachyandesitic magma. J Volcanol Geoth Res 84(1–2):103–123

Nash WP, Crecraft HR (1985) Partition coefficients for trace elements in silicic magmas. Geochim Cosmochim Acta 49:2309–2322

Pamukcu AS, Carley TL, Gualda GAR, Miller CF, Ferguson CA (2013) The evolution of the peach spring giant magma body: evidence from accessory mineral textures and compositions, bulk pumice and glass geochemistry, and rhyolite-MELTS modeling. J Petrol 54(6):1109–1148

Pe-Piper G, Piper DJW (2002) The igneous rocks of Greece. Gebrüder Borntreager, Berlin

Riciputi LR (1991) Petrology and Nd, Sr and Pb isotopes of the central San Juan caldera cluster, Colorado. PhD Thesis, University of Wisconsin Madison

Ridolfi F, Renzulli A, Puerini M (2010) Stability and chemical equilibrium of amphibole in calc-alkaline magmas: an overview, new thermobarometric formulations and application to subduction-related volcanoes. Contrib Miner Petrol 160(1):45–66

Rollinson HR (1993) Using geochemical data: evaluation, presentation and interpretation. Pearson Education Limited, Harlow

Shaw DM (1970) Trace element fractionation during anatexis. Geochim Cosmochim Acta 34:237–243

Steven TA, Lipman PW (1976) Calderas of the San Juan volcanic field, southwestern Colorado. US Geol Surv Prof Pap 958:1–35

Troll VR, Schmincke HU (2002) Magma mixing and crustal recycling recorded in ternary feldspar from compositionally zoned peralkaline Ignimbrite 'A', Gran Canaria, Canary Islands. J Petrol 43(2):243–270

Turnbull R, Weaver S, Tulloch A, Cole J, Handler M, Ireland T (2010) Field and geochemical constraints on Mafic-Felsic interactions, and processes in high-level arc magma chambers: an example from the Halfmoon Pluton, New Zealand. J Petrol 51(7):1477–1505

Whitney JA (1988) The origin of granite: the role and source of water in the evolution of granitic magmas. Geol Soc Am Bull 100(12):1886–1897

Whitney JA, Dorais MJ, Stormer JC, Kline SW, Matty DJ (1988) Magmatic conditions and development of chemical zonation in the Carpenter Ridge Tuff, Central San Juan volcanic field, Colorado. Am J Sci 288-A:16–44

Wiesmaier S, Troll VR, Carracedo JC, Ellam RM, Bindeman I, Wolff JA (2012) Bimodality of Lavas in the Teide-Pico Viejo Succession in Tenerife, Äîthe Role of Crustal Melting in the Origin of Recent Phonolites. J Petrol 53(12):2465–2495

Winter JD (2001) An introduction to igneous and metamorphic petrology. Prentice-Hall, Englewood Cliffs

Wolff JA, Worner G, Blake S (1990) Gradients in physical parameters in zoned felsic magma bodies: implications for evolution and eruptive withdrawal. J Volcanol Geoth Res 43:37–55

Worner G, Schmincke H-U (1984a) Petrogenesis of the Laacher See tephra. J Petrol 25:836–851

Worner G, Schmincke HU (1984b) Mineralogical and chemical zonation of the Laacher See Tephra sequence (East Eifel, W. Germany). J Petrol 25(4):805–835

Worner G, Staudigel H, Zindler A (1985) Isotopic constraints on open system evolution of the Laacher See magma chamber (Eifel, West Germany). Earth Planet Sci Lett 75(1):37–49

Zhang Y, Cherniak DJ (2010) Diffusion in minerals and melts: theoretical background. In: Zhang Y, Cherniak DJ (eds) Diffusion in minerals and melts. Rev Mineral Geochem 72:5–60